Integration Of Strength and Process Modelling of Friction-Stir-Welded Fuselage Panels

Published in:
Journal of Aerospace Computing, Information, and Communication

Document Version:
Peer reviewed version

Queen's University Belfast - Research Portal:
[Link to publication record in Queen's University Belfast Research Portal](#)

The Integration of Strength and Process Modeling of Friction-Stir-Welded Fuselage Panels

A. Murphy[*], M. Price[†] and R. Curran[‡]

Centre of Excellence for Integrated Aircraft Technologies, Queen's University Belfast, N. Ireland, U.K.

P. Wang [§]

Schlumberger, Stonehouse Technology Centre, Gloucestershire, UK.

In order to reduce potential uncertainties and conservatism in welded panel analysis procedures, understanding of the relationships between welding process parameters and static strength is required. The aim of this study is to determine and characterize the key process induced properties of advanced welding assembly methods on stiffened panel local buckling and collapse performance. To this end, an in-depth experimental and computational study of the static strength of a friction stir welded fuselage skin-stiffener panel subjected to compression loading has been undertaken. Four welding process effects, viz. the weld joint width, the width of the weld Heat Affected Zone, the strength of material within the weld Heat Affected Zone and the magnitude of welding induced residual stress, are investigated. A fractional factorial experiment design method (Taguchi) has been applied to identify the relative importance of each welding process effect and investigate

---

[*] Lecturer, School of Mechanical and Aerospace Engineering, Ashby Building, Belfast. BT9 5AH Northern Ireland, MAIAA.

[†] Senior Lecturer, School of Mechanical and Aerospace Engineering, Ashby Building, Belfast. BT9 5AH Northern Ireland, MAIAA, AIAA Aircraft Design Technical Committee Member.

[‡] Lecturer, School of Mechanical and Aerospace Engineering, Ashby Building, Belfast. BT9 5AH Northern Ireland, MAIAA, AIAA Economics Technical Committee Member.

[§] Engineer, Schlumberger – Stonehouse Technology Centre, Stroudwater Business Park, Gloucestershire. GL10 3SX England.

effect interactions on both local skin buckling and crippling collapse performance. For the identified dominant welding process effects, parametric studies have been undertaken to identify critical welding process effect magnitudes and boundaries. The studies have shown that local skin buckling is principally influenced by the magnitude of welding induced residual stress and that the strength of material in the Heat Affected Zone and the magnitude of the welding induced residual stress have the greatest influence on crippling collapse behavior.

I.   Introduction

To reduce aircraft acquisition and lifecycle costs airframe manufacturers are constantly considering new materials and advanced processing technologies. Typically, the skin and stiffener components of metallic aircraft primary structure are riveted together. Advanced fabrication processes such as laser beam welding[1] and friction stir welding[2] have the potential of significantly lower assembly times, resulting in lower manufacturing costs and higher productivity[3-4]. Additional potential lies with increased structural efficiency through the optimal placement of structural material and the elimination of fasteners. Although the potential of welding is recognized with laser beam welded panels on the Airbus 318 and 380 and friction stir welded panels on the Eclipse 500, there are still major issues to be addressed.

Significant thermal behavior, elastic- and plastic-deformation and metallurgical property changes occur simultaneously in the proposed welding techniques. Methods for strength analysis and design are currently under development[5-10], as well as manufacturing process parameter optimization for reliable welds[11-18] with minimum distortion. Current strength analysis methods apply empirically determined general knock down factors which account for all welding effects. This approach is permitting the introduction of welding to aircraft stiffened panel assembly, but

is limited and will not allow combined optimization of the manufacturing process and the structural strength performance.

The major limitation for fully optimized implementation of these advanced processes to actual manufacturing of aircraft structures is the lack of fundamental knowledge on the linkages between welding process parameters and the resultant induced or modified panel properties, and the consequence of these welding process effects on strength performance of the fabricated structure. As a result of the incomplete knowledge uncertainties remain in analysis procedures for performance. For these new manufacturing processes, fully integrated structural and process design is required to meet future project structural efficiency levels while maintaining manufacturing quality and reduced manufacturing cost.

The aim of this study is to determine and characterize the key manufacturing process effects of friction stir welding on stiffened panel local skin buckling and crippling collapse performance. To this end an in-depth experimental and computational study of the static strength of a friction stir welded fuselage skin-stiffener panel subjected to compression loading has been undertaken. Four welding process effects, namely, the weld joint width, the width of the weld Heat Affected Zone, the strength of material within the weld Heat Affected Zone and the magnitude of residual stress induced by the welding process, are investigated.

The friction stir welding process is a solid state joining technique. The process utilizes local frictional heating to produce continuous solid-state seams. The process joins material by plasticizing and then consolidating the material around the weld line. A cylindrical, shouldered tool with a profiled probe or pin is rotated and slowly plunged into the workpiece at the start of the weld line. The probe continues rotating and traverses forward in the direction of welding. Frictional heat is generated between the wear resistant tool and the material of the workpiece. As

the probe proceeds, the friction heats the surrounding material and rapidly produces a plasticized zone around the probe. This heat causes the workpiece to soften to a temperature below that of the material melting temperature and typically within the material's forging temperature range. As the tool moves forward metal flows to the back of the tool where it is extruded/forged behind the tool. It then consolidates and cools to form the bond. To produce a full-penetration groove weld in a butt joint, the bottom of the tool must be close to the bottom of the workpiece. In order to make a lap joint, the bottom of the tool must only extend through the bottom of the top sheet and into the bottom sheet, creating a metallic bond between the two sheets. A schematic drawing of the lap joint welding process is shown in Fig. 1. The weld is left in a fine-grained, hot-worked condition with no entrapped oxides or gas porosity. A benefit of this welding process is that it allows welds to be made on standard aircraft production aluminum alloys, which cannot be readily laser beam welded. In addition, friction stir welding is a robust, process tolerant technique. It has the advantage that many of the welding parameters, e.g. tool design, rotation speed and translation speed, can be controlled in a precise manner, thus controlling the energy input into the system.

Although there are a number of limitations inherent with this process, including slower translation speeds than for fusion welding, a keyhole at the end of each weld line and rigid clamping required for all workpieces, friction stir welding has already found its way into various industrial applications. Examples include large marine panels with welding lengths up to 14.5 m at Sapa in Sweden[19], cargo and ramp floor sections at Boeing[19] and space shuttle external tanks and rocket boosters at NASA[20]. Recently, friction stir welding has been considered by major airframe manufacturers including Boeing, Airbus and Bombardier to replace riveting in landing gear doors, cabin assemblies and stiffened fuselage panels. Significant research has been carried

out to develop an understanding of joint properties of friction stir welds[11-18]. However, existing methods for stiffened panel design are based on conventional manufacturing techniques such as riveting; limited experience has been accumulated for friction stir welded stiffened panels[8-10].

In the present study, the buckling and post buckling response of a single stiffener friction stir welded panel has been investigated experimentally and computationally. In the experimental study, three identical specimens were manufactured and tested to aid in the validation of the computational Finite Element predictions. In the Finite Element study, a fractional factorial experiment design method, the Taguchi method[21], was integrated in a sensitivity study to identify the relative importance of the four welding process effects. The following section briefly introduces the validation experimental set-up. The succeeding section then outlines the computational Finite Element analysis methods applied. This is followed by details on the fractional factorial experiment design method, and the welding process effect sensitivity studies. The computational and experimental results are then presented and discussed before the paper concludes with the determined relationships between welding process effects and structural performance.

II. Validation Experiments

The analysis work is validated on a single stiffener crippling specimen design, with a Z-section stringer stiffener (7075-T76511 extrusion) and a flat skin base (2024-T3). The specimen skin thickness and stringer dimensions are representative of panel structure found on the lower fuselage belly of mid-sized commercial transport aircraft, Fig. 2. Three specimens, labeled as FSW-1, FSW-2 and FSW-3, were manufactured and tested. The welding process parameters including tool design, tool tilt angle, rotation speed, translation speed, translation pressure, forging pressure and welding fixturing details are proprietary.

The design philosophy of the welded panels was the same as for riveted panels, that is to say, skin local buckling occurring at a percentage of the ultimate load, with subsequent post buckling failure due to buckling collapse of the stiffeners. Within the post-buckling range as with riveted designs the stiffener plus an effective width of skin[22] is assumed to act as a column, independent of the buckled skin. Therefore, no weld joint failure should occur before the ultimate collapse load, this is similar in philosophy to removing the potential for inter rivet buckling in a riveted panel design.

The three specimens were tested to failure when subjected to compression using a 250 kN displacement-controlled hydraulic testing machine. 25.4 mm thick Cerrobend (low melting point alloy) bases were cast on to the top and bottom ends of the specimens, producing a fully-clamped boundary condition at each end, Fig. 2. The ends were machined flat and perpendicular to the skin to ensure that uniform compression load was applied. Two LVDTs, one either side of the specimen, were used to measure the end-shortening. Uniaxial strain gauges were applied back to back at the mid-point of the free edge of specimen FSW-2 in order to determine initial buckling behavior. The tests were carried out by applying the compression load monotonically at a rate of approximately 10 kN/min until the specimens could not sustain further loading. Strain data and displacement readings were recorded at 4-second intervals.

III.   Computational Analysis

As noted previously, the friction stir welding process involves significant mechanical, thermal and metallurgical property changes. Hence panel and joint properties will include modified geometry, material properties, induced residual stresses and geometric imperfections. Considering the number of potential parameters the development of full empirical relationships would not be cost effective. Consequently a detailed validated study was carried out on one

configuration and statistical methods used in combination with models of a wider range of parameter values to establish trends and impacts. Using the Finite Element method and employing non-linear material and geometric analysis procedures, it is possible to model the local buckling and post buckling failure behavior of stiffened panels[23, 24] and to include for process effects such as the Heat Affected Zone and weld joint width.

The following sub-sections outline the modeling details applied in the succeeding Finite Element analysis:

A. Idealization

The idealization approach adopted represents the stiffener web and flanges and the panel skin as an assemblage of shell elements. This approach is essential to enable the crippling failure mode of the structure to be simulated[23, 24]. A number of idealizations for the skin-stiffener weld joint have been assessed[10]. Figure 3 schematically outlines the most appropriate representation, in which the nodes in the skin and stiffener weld joint area (w_{weld}) are connected with rigid links and the contact condition between the unwelded skin and stiffener flange is modeled using uni-axial gap elements, GAPUNI[26]. For the pad-up, the thicker part of the skin, Fig. 2, the shell elements that represent the pad-up are offset so that their bottom surfaces coincide with the skin bottom surface.

B. Element Selection

To enable element selection a series of mesh convergence studies were undertaken. The buckling behavior of uniformly compressed rectangular plates with geometries and boundary conditions designed to replicate those of the structure under investigation were carried out. Each analysis set was developed such that a theoretical buckling calculation could be preformed[27]. The performance of five ABAQUS elements were assessed based on convergence with

corresponding theoretical behavior with increasing mesh densities. Based on these analyses the first-order curved quadrilateral 4-noded finite strain general-purpose shell element, S4R[26] were selected.

C. Loads and boundary conditions

The loads and boundary conditions applied to the Finite Element models were designed to be as representative of the experimental test setup as possible, with the same loading and boundary conditions applied to each model. A uniform axial displacement was applied to one end of the model with the axial displacement at the opposite end restrained. Out-of-plane displacements of the nodes within the areas that were cast in Cerrobend in the experimental test were also restrained, Fig. 2.

D. Material Properties

Parent (unwelded) material properties were obtained from compression material coupon tests. The test coupons were cut from the same material batch as the components from which the validation specimens were manufactured. Stress-strain curves obtained from the coupon tests are shown in Fig. 4. The full material stress-strain curves were incorporated into the finite element analysis models using the 'classical metal plasticity' constitutive theory available within the ABAQUS material library[26].

E. Solution Procedure

For each analysis a two phased Finite Element solution procedure was used. The first phase analysis starts with the perfect specimen geometry, the welding induced residual stresses are applied and a linear equilibrium analysis is used to generate a specimen model containing manufacturing imperfections (stress plus geometric imperfections). The second phase analysis

8

starts with this imperfect model and a full non-linear material and geometric post buckling analysis is then performed using the incremental-iterative Newton-Raphson solution procedure[26]. This two phase approach is required so the full analysis starts with an imperfect model which eliminates bifurcation points from the non-linear solution path, allowing a complete buckling and collapse structural analysis.

IV.   Welding process effects

In the present study, four welding process effects are investigated:

1. Weld joint width (w_{weld}) – this is the lateral width of the physically joined skin and stiffener flange material, Fig. 5.

2. Heat Affected Zone (HAZ) width (z) – the HAZ is the region surrounding the weld in which the greatest change in metallurgical and material property occurs. The distance the HAZ extends from the weld is defined as the HAZ width, Fig. 5.

3. The strength of material within the weld HAZ (k_z) – with most metals used in fabrication, with the exception of steel, the HAZ material has lower strength than the parent metal[25]. The factor k_z relates the strength of HAZ material to the parent material (unwelded material), k_Z being equal to the ratio of HAZ material proof stress to parent material proof stress.

4. Magnitude of residual stresses (σ_{res}) – the induced welding residual stresses (due to the welding heating and softening cycle) are typically defined in relation to the material proof stress.

The following sub-sections outline the modeling details applied in the succeeding Finite Element analysis related to the welding process effects under investigation. The sub-sections also outline the range of examined welding process effects.

F. Weld Joint Width

A macrograph of a typical validation specimen weld section is presented in Fig. 6. The width of the weld joint is approximately 3 mm. Five weld joint widths, viz. w_{weld} = 2.0, 2.5, 3.0, 3.5 and 4.0 mm, are to be considered in the computational study. The weld joint width is directly related to the weld tool pin diameter. The selected range enables the examination of tool design on the static strength performance of the structure.

G. Heat Affected Zone (HAZ) width

Normally, the width of the reduced strength zone extends each side of the weld and the width is primarily influenced by the welding parameters and workpiece material. Conventional analysis methods, which cover fusion welding[28, 29], tend to predict large HAZ widths. Research on friction stir welded joints in aluminium[12, 13, 15, 30] suggests that the extent of the HAZ is relatively concentrated, normally of the same magnitude as the weld joint width. In light of this, HAZ width in the computational study are varied z = 0.0, 1.0, 2.0 and 3.0 mm. This welding effect relates to the heat input of the welding process and is therefore a result of weld tool design (pin and shoulder geometry), rotation / translation speed and forging / translation pressure. The selected range enables the examination of welding energy input on the static strength performance of the structure.

H. HAZ material strength

The material within the HAZ generally has lower strength than the parent material and for design the change in strength is generally accounted for by locally reducing the material properties or thickness of material (static strength analysis only). Test results of mechanical properties of friction stir welds[11-18] reveals that, for aluminum alloys, in the transverse direction, the ultimate tensile strength varies from 41% to 106% the parent material. Limited results for

mechanical properties of aluminium welds in the longitudinal direction have been published, which is the loading direction in this application, Fig. 2. In the present research, the material strength in the HAZ is varied in the range of 50 to 125% of the parent material to ensure a broad coverage of the range. In the Finite Element analysis the stress-strain relationships for the HAZ materials is modeled using Ramberg-Osgood. The yield stresses ($\sigma_{0.1\%}$ and $\sigma_{0.2\%}$) are adjusted by the appropriate percentage, with the elastic modulus and the knee factor of the Ramberg-Osgood relationship unchanged. Again this welding effect relates to the heat input of the welding process, and is therefore dependant on weld tool design, rotation / translation speed and forging / translation pressures.

I. Residual stresses

It is well established that the fusion welding process will introduce residual stress fields and associated geometric induced distortions[31]. The magnitude and distribution of the residual stresses and the magnitude of the geometric distortions are governed by welding process parameters and in addition workpiece pre and post welding temperature control. Residual stress distribution in fusion welded stiffened panels in the longitudinal direction is sufficiently well documented by Masubuchi, Ref. 31. Measurements of magnitude and distribution of residual stresses adjacent to friction stir welds have recently been carried out by a number of researchers[32, 33] on aluminum 2024 plate butt welds. Values of maximum longitudinal residual stress in the weld zone ranging from 40% to 85% of the parent material's yield strength are reported.

In the present study, the longitudinal residual stress distributions in the skin and stiffener do not vary in the longitudinal direction as the test specimens were cut from the centre section of a continuous friction stir welded workpiece. The longitudinal residual stresses also remain constant

through the thickness as the skin thickness is relatively small in comparison to the workpiece global dimensions. Transverse residual stresses are assumed small in comparison with the longitudinal residual stresses and their effects are therefore not modeled. Fig. 7 depicts how the residual stresses are distributed in the succeeding Finite Element analysis: tensile residual stresses are applied to the width of the weld joint, with magnitude varying from zero (no residual stress) to as high as the proportional limit of the HAZ material. These tensile stresses are then balanced by uniform compressive stresses distributed over the remaining skin and stringer section, Fig. 7.

It is worth noting that the residual stress distribution shown in Fig. 7(b) is not in equilibrium when introduced to the Finite Element models since the stresses are applied in different planes in space. An initial linear analysis is carried out in order to establish static equilibrium (force and moment) before any external load is applied. The equilibrium calculation generates a distorted structure and a slightly modified stress state. This combined stressed and distorted state obtained from this initial analysis is used as the initial condition for the full collapse analysis. The induced residual stresses relates to the heat input of the welding process and the process setup including workpiece temperature control and fixturing (as fixturing potentially acts as an effective heat sink).

V. Design of Experiment (Taguchi Method)

When considering four varying input factors simultaneously, the interpretation of results can be difficult due to the problem complexity and interaction between the factors. The technique of investigating all possible conditions involving multiple input factors is referred to as factorial design. For a full factorial design the number of possible designs (analysis simulations) N is L^m where L is the number of levels for each factor and m the number of factors. Thus, in the present

study for a full factorial design, considering each of the four factors at only four levels would require 256 analysis simulations ($4^4 = 256$). The Taguchi method, which is essentially a fractional factorial experiment design method, has been employed in the present study to govern the analysis simulations, estimate the relative contributions of the individual welding process effects (input factors) and investigate interactions. The use of this method has reduced the initial computational cost significantly, allowing second stage parametric studies examining the dominant input factors.

In the Taguchi method, a special set of orthogonal arrays are used and all input factors are treated as discrete. Each row in the orthogonal array represents a Finite Element simulation, with factor levels indicated by the numbers in the row. Vertical columns correspond to specific factors. Once the orthogonal array has been determined, simulations are carried out to predict the specimen local skin buckling and collapse loads. Based on the simulation results (local skin buckling and collapse loads) an 'Analysis of Means' is carried out to identify the dominant factors influencing the loads. Again based on the same simulation results an 'Analysis of Variance' is undertaken to determine the relative contributions of each factor to the predicted loads. Using the Taguchi method in the present case, only 8 analysis simulations are required to identify the dominant factors and their potential interactions, Table 2. This increases the available computational resources and time to study the dominant factors, allowing more factor levels to be considered and therefore a full characterization of factor sensitivity.

VI.   Results

J. Experimental results

Experimental data, including buckling and collapse loads, for the three validation specimens are presented in Table 1. Figure 8 depicts specimen FSW-2 deformed shape after ultimate load.

13

For each specimen tested, weld joint integrity was maintained throughout local skin buckling, post-buckling and ultimately overall specimen crippling collapse.

The load-displacement response of the specimen validation tests is plotted in Fig. 9. A similar structural response was found for each validation specimen, with each failing in a crippling mode, Fig. 8. The response curves show increased scatter as the collapse load is approached. However, all experimental crippling loads were within 2.4% of each other.

The predicted load-displacement response from a perfect specimen Finite Element simulation representing no welding process effects is also plotted in Fig. 9. The basic Finite Element model predicts a specimen crippling failure similar to the experimental modes but under predicts the minimum experimental failure load by 2.1%.

Examining the load-displacement curves, the simulation predicts the theoretical pre local skin buckling stiffness, which the validation specimens fail to match. The validation specimen stiffness is on average 10.9% lower than the calculated theoretical stiffness assuming no welding process effects. This suggests that the welding process effects reduce the validation specimen's initial stiffness response.

Generally, the Finite Element prediction is reasonably good, with a maximum difference in ultimate specimen load of 4.4%. However, to understand the variation in the experimental and computational results and therefore remove or reduce potential uncertainties from prediction analysis, the definition and characterization of the dominant welding process effects must be undertaken.

K. Computational results

1. Dominant welding process effect(s) (Analysis of Means)

To identify the dominant welding effect(s) a series of analyses based on a Taguchi special orthogonal array were undertaken with each of the four manufacturing effects examined at only two levels. One value representing a 'large' or 'high' magnitude of the particular welding process effect and the other value representing a 'small' or 'low' magnitude of the particular welding process effect, Table 2. These bounding values have been selected based on data from previous and current research programs on friction stir welding and laser beam welding of aircraft stiffened panels and relevant data found in the open literature.

Interaction between the factors (welding process effects) is mixed with direct factor affects. To assess the influence of potential interactions, two interactions are included within the special orthogonal array, Table 2. The first interaction considers the relationship between HAZ material strength and weld joint width, the second considers the relationship between HAZ material strength and HAZ width. Interactions with other combinations of the four welding process effects are considered less significant, and are therefore not examined in detail at this stage.

Using the predicted local skin buckling and crippling failure loads from the 8 Finite Element simulations as outlined in Table 2, an 'Analysis of Means' was carried out. The influence of the four individual welding process effects on specimen local skin buckling and crippling collapse loads is plotted in Fig. 10a and Fig. 10b respectively. Results obtained from the interaction analysis of the simulation results is plotted in Fig. 11a and 11b, again for specimen local skin buckling and crippling collapse loads respectively.

First focusing on individual welding process effects, it is seen that, for the analyzed range of factors, residual stress has the greatest influence on the local skin buckling performance, Fig.

10a. Considering the crippling collapse load, Fig. 10b, the residual stress and the HAZ material strength have the greatest influence on performance.

Considering interaction for local skin buckling, Fig. 11a, the lines A1 and A2 neither intersect nor are they parallel to each other. This implies that interaction between weld joint width (Factor A) and HAZ material strength (Factor C) are slight in the studied factor range. Also lines B1 and B2 neither intersect nor are parallel to each other, again implying that the interaction between the HAZ width (Factor B) and the HAZ material strength (Factor C) are again slight in the studied range.

Examining the interactions for crippling collapse, Fig. 11b, lines A1 and A2 and lines B1 and B2 intersect respectively. This indicates that, in terms of the collapse load, weld joint width (Factor A) and HAZ material strength (Factor C) and HAZ width (Factor B) and HAZ material strength (Factor C) interact with each other respectively. The existence of these interactions implies that, for crippling collapse, it is not appropriate to evaluate the influence of these welding process effects individually, and that the interactions should be considered along with the individual factor affects.

2. Relative contributions of welding process effects (Analysis of Variance)

Using the predicted local skin buckling and crippling collapse failure loads from the 8 Finite Element simulations, an 'Analysis of Variance' was carried out to identify the relative significance of the individual factors and their interactions. Examining the results of the analysis, Table 3, for local skin buckling, the magnitude of welding induced residual stress is again identified as the dominant welding process effect, with an individual contribution of approximately 75%. Considering crippling collapse the HAZ material strength and the welding

induced residual stresses have the most significant influence of the four evaluated welding process effects, with a combined total contribution of approximately 80%.

Finally, it is important to note that these initial results identifying the dominant welding process effect(s) and their level of influence on static strength are not fully generic, and are influenced by the range of effect magnitudes analyzed. It is therefore again noted that the selected range of effect magnitudes is broad and not particular to a single processing configuration. Further analysis is currently underway considering particular welding setups, based on both experimental data and computational process modeling results.

3. Dominant welding process effect sensitivity studies (Parametric study)

Having identified the dominant welding process effect(s) on both local skin buckling and crippling collapse, a series of parametric studies are now undertaken to determine the sensitivity of the relationships and identify critical magnitudes and boundaries.

For the local skin buckling parametric study the magnitude of the welding induced residual stress is varied and the weld joint width held constant at 3 mm, equaling the experimentally measured width. The influence of the HAZ width and HAZ material strength are suppressed by setting the HAZ material strength equal to the parent material strength. For the crippling collapse parametric study the magnitude of the welding induced residual stress and the HAZ material strength is varied. The weld joint width is again held constant at 3 mm. Finally, the HAZ width is set constant at 3 mm to allow the maximum influence of the HAZ material strength factor to be demonstrated.

The effect of initial residual stress magnitude on specimen local skin buckling performance is shown in Fig. 12. The figure also presents the maximum out-of-plane magnitude of the induced geometric imperfection due to the applied residual stress imperfection. There is a clear linear

relationship between the magnitude of applied residual stress and the resultant magnitude of induced geometric imperfection. It is also worth noting that the resultant geometric imperfection mode is independent of the residual stress magnitude, with all predicted geometric imperfections of the same wave form, Fig. 14.

Considering local skin buckling load, Fig. 12, the load decreases continuously with higher magnitudes of initial residual stress and the associated resultant geometric imperfections. However, the reduction in performance is not linear throughout the range of magnitudes. For initial magnitudes of residual stress below 15% (of the material proportional limit) the reduction is approximately linear and approximately at a rate of -0.03 kN per 1% increase in residual stress. Between 15 and 20% there is a step change in performance and between 20% and 40% the reduction is approximately linear and at a rate of -0.04 kN per 1%. For initial residual stress magnitudes greater than 60% the local buckling performance appears to be less sensitive, with a lower rate of reduction for a given increase in residual stress. With a residual stress of 100% the proportional limit, the specimen local skin buckling performance is approximately 15% lower than that exhibited when zero residual stress is present.

The predicted local skin buckling curves are not perfectly smooth due to a limitation of the method used to define initial buckling. In the present study, the average strain method[34] is used both in the experimental and computational analysis, therefore allowing comparison of the results. The method plots compression load versus mid-plane strain and buckling is defined to have occurred at the inflection point, Fig. 13. The strain data used for each experimental and computational calculation is taken at the same location, i.e. at the strain gauge location – mid-point of the free edge of the specimen. The method therefore only considers a single point on the plate and considering the non-localized behavior of buckling the analysis results are highly

dependent on the gauge location and the initial buckling wave formation, particularly the relative locations of the measurement and initial buckling wave crests.

The parametric study results for crippling collapse performance are shown in Fig. 14. It is seen that for a specific magnitude and distribution of residual stresses, the specimens collapse load increases with higher HAZ material strength. However, for a specific value of HAZ material strength, the response is complicated when varying the magnitude of the residual stress. For magnitudes of residual stress between 0 and 12% (of the proportional limit), the specimen collapse load changes little. However, when the magnitude of the tensile residual stress is increased to between 14 and 16%, the specimen collapse load increases by between 0.6 and 0.9% depending on HAZ material strength. With a further increase in residual stress magnitude, specimen collapse load drops by between 5.4 and 5.7% depending on HAZ material strength and is thereafter significantly less sensitive to increased residual stress magnitude.

Further analysis reveals that the characteristic response of the specimen collapse load versus residual stress magnitude relates to the specimen failure mode. Only the magnitude of the initial geometric imperfection changes with increased residual stress magnitude, the mode shape does not change, Fig. 14. However, the increase in geometric imperfection magnitude does induce a change in the local skin buckling mode between 12 and 14%, and again between 16 and 18%, Fig. 14. The change in local buckling mode between 12 and 14% helps explain the step change in local buckling performance found between 15% and 20% in the previous results. Considering specimen crippling collapse performance, both changes in local skin buckling mode result in changes in the specimen crippling mode, Fig. 14. These changes in failure mode are accompanied with step changes in collapse load, which are clearly depicted in the graph, Fig. 14.

VII. Conclusion

The aim of this study was to determine and characterize the key manufacturing process effects of friction stir welding on stiffened panel local buckling and crippling performance. This was achieved by carrying out an in-depth experimental and computational study of the static strength of a friction stir welded fuselage skin-stiffener panel. Four welding process effects were investigated, viz. the weld joint width, the width of the weld Heat Affected Zone, the strength of material within the weld Heat Affected Zone and the magnitude of residual stress induced by the welding process. Three validation specimens were tested to failure and the experimental program has demonstrated the potential static strength of friction stir welded skin-stringer joints for aircraft panel structure. For each specimen tested, weld joint integrity was maintained throughout local skin buckling, post buckling and ultimate crippling failure.

Utilizing a fractional factorial experiment design method and the Finite Element method the dominant welding process effects for local skin buckling and crippling collapse have been identified. Additionally, for the identified as significant welding process effects, parametric studies have been used to determine the sensitivity of the relationships and identify critical magnitudes and boundaries. The results have shown that, local skin buckling is principally influenced by the magnitude of the welding induced residual stress and resultant geometric imperfections. Considering crippling collapse the HAZ material strength and the welding induced residual stresses have the most significant influence of the four evaluated welding process effects.

For the structural configuration examined herein, local skin buckling performance decreases continuously with higher magnitudes of initial residual stress. The reduction in performance is greater at lower magnitudes of residual stress than at higher magnitudes. Over the total range of

magnitudes possible, there was a total decrease in specimen local skin buckling performance of approximately 15%. Considering specimen collapse performance, varying magnitudes of initial residual stress result in varying local buckling modes and ultimately failure modes and resultant loads. For the structural configuration examined herein, a change in local buckling and failure mode resulted in a step change in collapse performance of approximately 6%. Relating this impact to welding process design, clearly the optimization of a welding process (selection of weld tool, rotation / translation speed, forging / translation pressure) which results in a maximum longitudinal residual stress lower than 20% material yield strength will benefit structural behavior and therefore weight.

Finally over the total range of HAZ material strengths and residual stresses examined within the parametric study, there was a variation in specimen crippling collapse performance of approximately 9%.

References

[1]Mendez, P. F., and Eagar T. W., "Welding Processes for Aeronautics," *Advanced Materials & Processes*, May 2001, pp. 39, 43.

[2]Midling, O. T., "Material flow behaviour and microstructural integrity of friction stir butt weldments," *Proceedings of the 4th International Conference on Aluminium Alloys*, Atlanta, 1994, pp. 451, 458.

[3]Irving, P., "End of the aircraft rivet-the coming of the welded aircraft," *Aerogram*, Vol. 10, No. 2, September 2001, pp. 31, 41.

[4]Zink, W., "Laser beam welding for aircraft structures," *Aeromat 2000*, Daimler Chrysler Aerospace Airbus, Bremen, 2000.

[5]Gibson, A., and Sterling, S., "A design and test programme involving welded sheet-stringer compression panels," *ICAS 1998*, Melbourne, Australia, August 1998, ICAS-98-7.7.4.

[6]Price, M., McClatchey, G., Gibson, A., Murphy, A., Curran, R., Ou, H., and Armstrong, C. G., "Design of Welded Aluminium Fuselage Panels for Improved fatigue Performance," *MetFab 2003*, Nottingham, September 2003.

[7]Lynch, F., Price, M., Murphy, A., Gibson, A., Poston, K., and Moore, G., "Analysis of Weld Configuration for Laser Welded Skin-Stringer Fuselage Sub-Panels in Compression," *Fourth International Conference on Thin-Walled Structures*, Loughborough, June 2004, pp. 145, 152.

[8]Dracup, B. J., and Arbegast, W. J., "Friction stir welding as a rivet replacement technology," *Proceedings of the 1999 SAE Aerospace Automated Fastening Conference & Exposition*, Memphis, October 5-7, 1999.

[9]Hoffman, E. K., Hafley, R. A., Wagner, J. A., Jegley, D. C., Pecquet, R. W., Blum, C. M., and Arbegast, W. J., "Compression Buckling Behaviour of Large-Scale Friction Stir Welded and Riveted 2090-T83 Al-Li Alloy Skin-Stiffener Panels," NASA/TM-2002-211770, August 2002.

[10]Murphy, A., Lynch, F., Price, M., and Wang, P., "The Static Strength Analysis of Friction Stir Welded Stiffened Panels for Primary Fuselage Structure," *ICAS 2004*, Yokohama, August 2004, ICAS-2004-5.6.3.

[11]Baumann, J. A., Lederich, R. J., Bolser, D. R., and Talwar, R., "Property characterization of 2024AL/7075AL bi-alloy friction stir welded joints," *Friction Stir Welding and Processing II -*

Proceedings of symposium sponsored by the Shaping and Forming Committee, Indianapolis, November 2001, pp. 199, 207.

[12]Liu, H. J., Fuji, H., Maeda, M., and Nogi, K., "Tensile properties and fracture locations of friction-stir-welded joints of 2017-T351 aluminium alloy," *Journal of Materials Processing Technology*, Vol. 142, No. 3, 2003, pp. 692, 696.

[13]Peel, M., Steuwer, A., Preuss, M., and Withers, P.J., "Microstructure, mechanical properties and residual stresses as a function of welding speed in aluminium AA5083 friction stir welds," *Acta Materialia*, Vol. 51, No. 16, 2003, pp. 4791, 4801.

[14]Lockwood, W. D., Tomaz, B., and Reynolds, A. P., "Mechanical response of friction stir welded AA2024: experiment and modeling," *Materials Science and Engineering A*, Vol. 323, No. 1-2, 2002, pp. 348, 353.

[15]Lee, W.B., Yeon, Y.M., and Jung, S.B., "The improvement of mechanical properties of friction-stir-welded A356 Al alloy," *Materials Science and Engineering A*, Vol. 355, No. 1-2, 2003, pp. 154, 159.

[16]Boz, M., and Kurt, A., "The influence of stirrer geometry on bonding and mechanical properties in friction stir welding process," *Materials & Design*, Vol. 24, No. 4, 2004, pp. 343, 347.

[17]Kwon, Y. J., Shigematsu, I., and Saito, N., "Mechanical properties of fine-grained aluminium alloy produced by friction stir process," *Scripta Materialia*, Vol. 49, No. 8, 2003, pp. 785, 789.

[18]Reynolds, A. P., Tang, W., Gnaupel-Herold, T., and Prask, H., "Structure, properties, and residual stress of 304L stainless steel friction stir welds," *Scripta Materialia*, Vol. 48, no. 9, 2003, pp. 1289, 1294.

[19]Kallee, S. W., "Invention, implementation and industrialization of friction stir weld," *First Eurostir Workshop*, Cambridge, UK; 2002.

[20]Bhat, B. N., Carter, R. W., Ding, R. J., Lawless, K. G., Nunes, A. C., Russell, C. K., and Shah, S. R., "Friction stir welding development at NASA - Marshall Space Flight Centre," *Friction Stir Welding and Processing - Proceedings of symposium sponsored by the Shaping and Forming Committee*, Indianapolis, November 2001, pp. 117, 127.

[21]Taguchi, G., *Introduction to Quality Engineering*, White Plains, NY, Asian Productivity Organization, 1986.

[22]Rhodes, J., and Walker, A. C., *Developments in thin-walled structures*, Applied science publisher, London, 1982, Chapter 4.

[23]Lynch, C., Murphy, A., Price, M., and Gibson, A., "The computational post buckling analysis of fuselage stiffened panels loaded in compression," *Thin-Walled Structures*, Vol. 42, No. 10, 2004, pp. 1445, 1464.

[24]Murphy, A., Price, M., Lynch, C., and Gibson, A., "The computational post buckling analysis of fuselage stiffened panels loaded in shear," *Thin-Walled Structures*, Vol. 43, No. 9, 2005, pp. 1455, 1474.

[25]Gourd, L. M., *Principles of Welding Technology*, 3rd ed., Arnold, London, 1995.

[26]Anonymous, *ABAQUS / Standard user's manual*, Hibbitt, Karlsson and Sorenson, 2000.

[27]Bulson, P. S., *The stability of flat plates*, 1st ed., Chatto & Windus, London, 1970.

[28]Anonymous, *Structural use of aluminium, part 1: Code of practice for design*, British Standard 8118, 1991.

[29]Anonymous, *Design of aluminium structures, part 1-1: General rules*, Eurocode 9, 1998.

[30]Uzun, H., Donne, C. D., Argagnotto, A., Ghidini, T., and Gambaro, C., "Friction stir welding of dissimilar Al 6013-T4 to X5CrNi18-10 stainless steel," *Materials & Design*, Vol. 26, 2005, pp. 41, 46.

[31]Masubuchi, K., *Analysis of welded structures*, Oxford, Pergamon Press, 1980.

[32]Bussu, G., and Irving, P. E., "The role of residual stress and heat affected zone properties on fatigue crack propagation in friction stir welded 2024-T351 aluminium joints," *International Journal of Fatigue*, Vol. 25, No. 1, 2003, pp. 77, 88.

[33]Staron, P., Koçak, M., Williams, S., and Wescott, A., "Residual stress in friction stir-welded Al sheets," *Physica B: Condensed Matter*, Vol. 350, No. 1-3, 2004, pp. 491, 493.

[34]Singer, J., Arbocz, J., and Weller, T., B*uckling experiments: experimental methods in buckling of thin-walled structures (Volume. 1)*, Chichester, England, John Wiley & Sons, 1998.
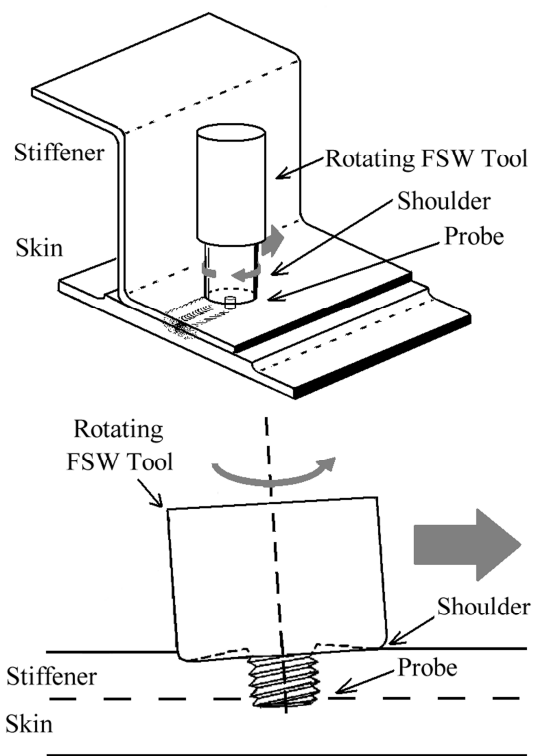
Figure 1. Friction stir welding. *The figure depicts the welding set-up for a skin-stiffener lap welding process.*
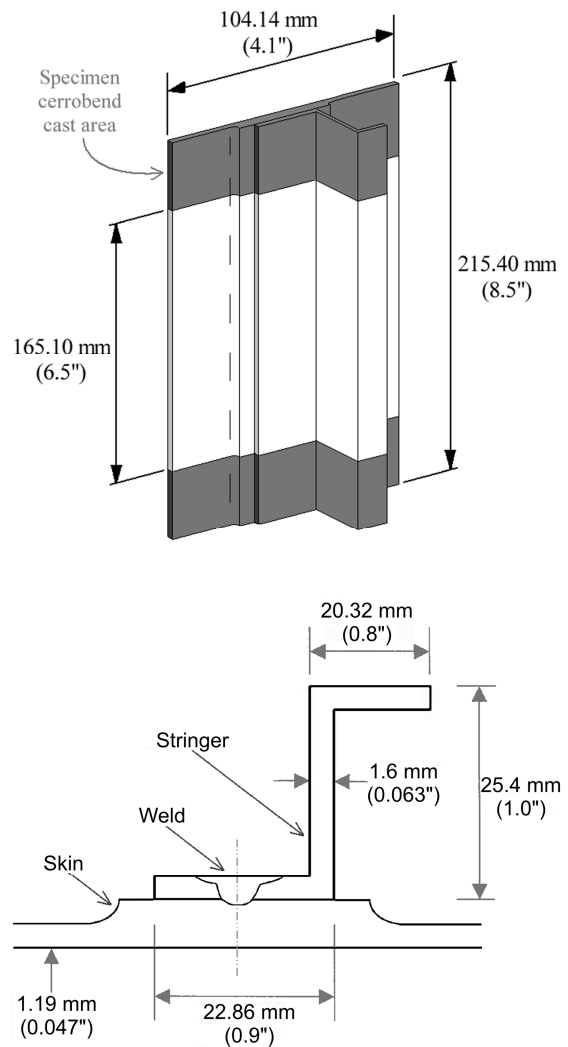
Figure 2. Specimen geometry. *The figure outlines the geometric details of the friction stir welded validation crippling specimens.*
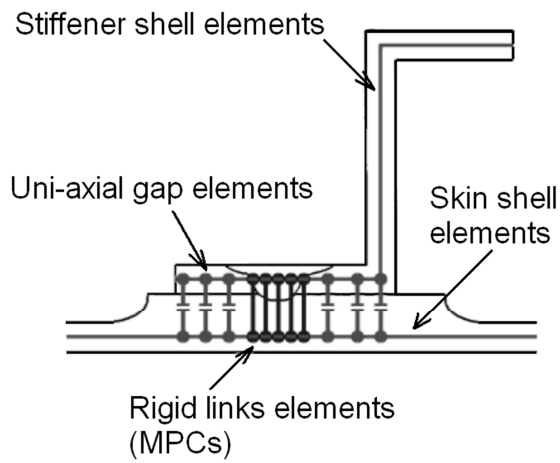
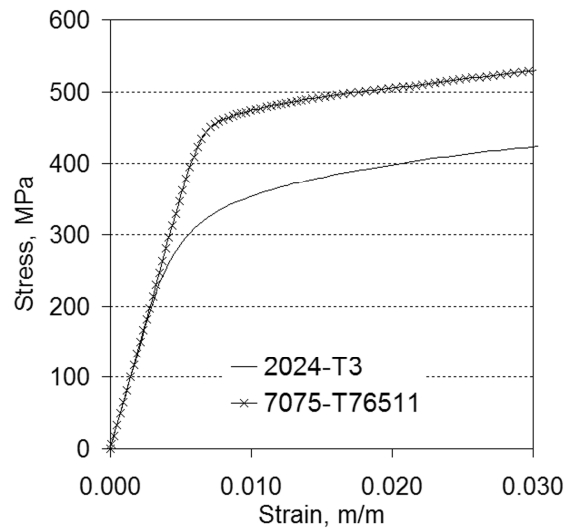**Figure 3. Weld joint idealization.** *The figure depicts the modeling idealization used for the welded lap joint.*

Figure 4. Material properties. *The graph presents the skin and stringer compression stress-strain coupon test data.*
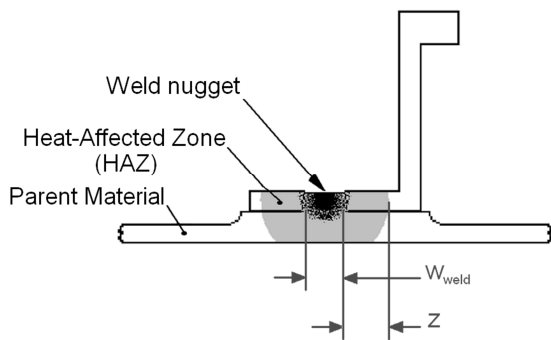
Figure 5. Weld cross-section. *The figure depicts the welding effects under investigation.*
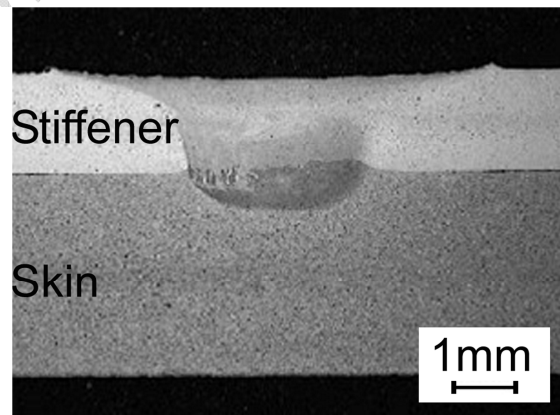
Figure 6. Macrograph of skin-stringer joint. *Macrograph of specimen skin-stiffener lap welded joint.*
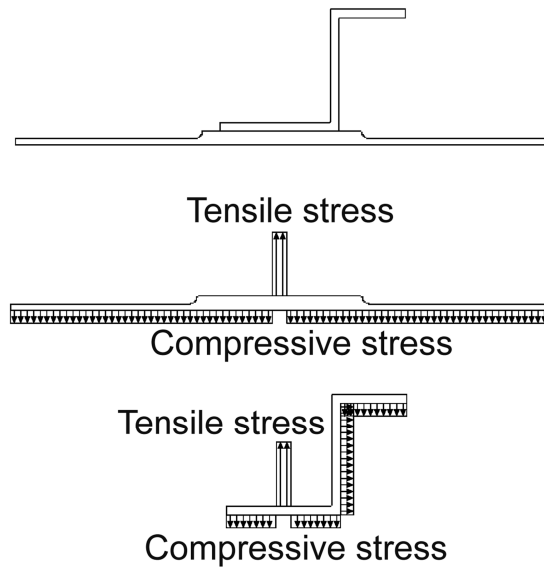
Figure 7. **Specimen residual stresses.** *The figure depicts the representation of longitudinal residual stresses in the welded specimen.*

Figure 8. **Validation specimen crippling.** *The figure illustrates the ultimate failure mode of validation specimen FSW-2 prior to the removal of applied loading.*
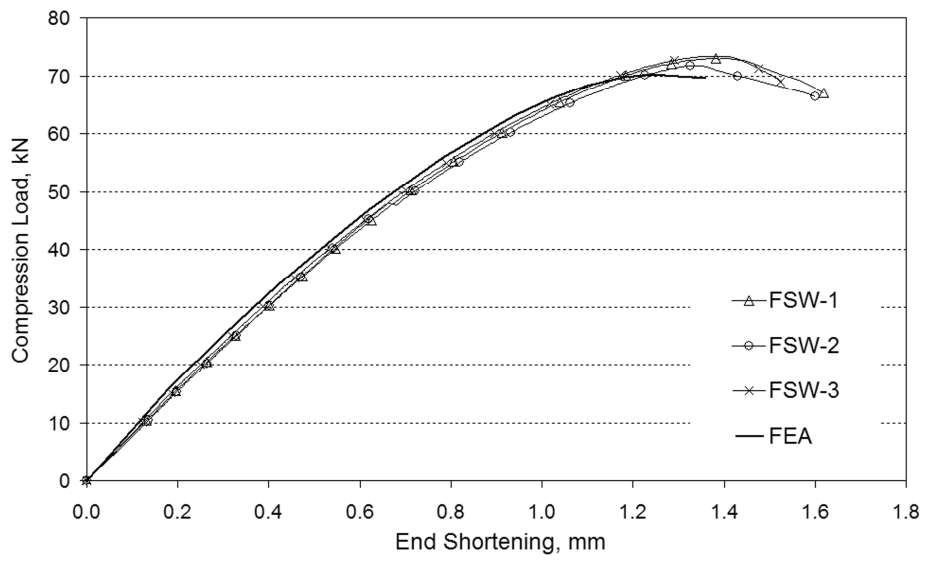
Figure 9. Load-displacement curves. *The figure presents the load-axial displacement curves for the 3 validation specimens and the Finite Element analysis which considers no welding process effects.*
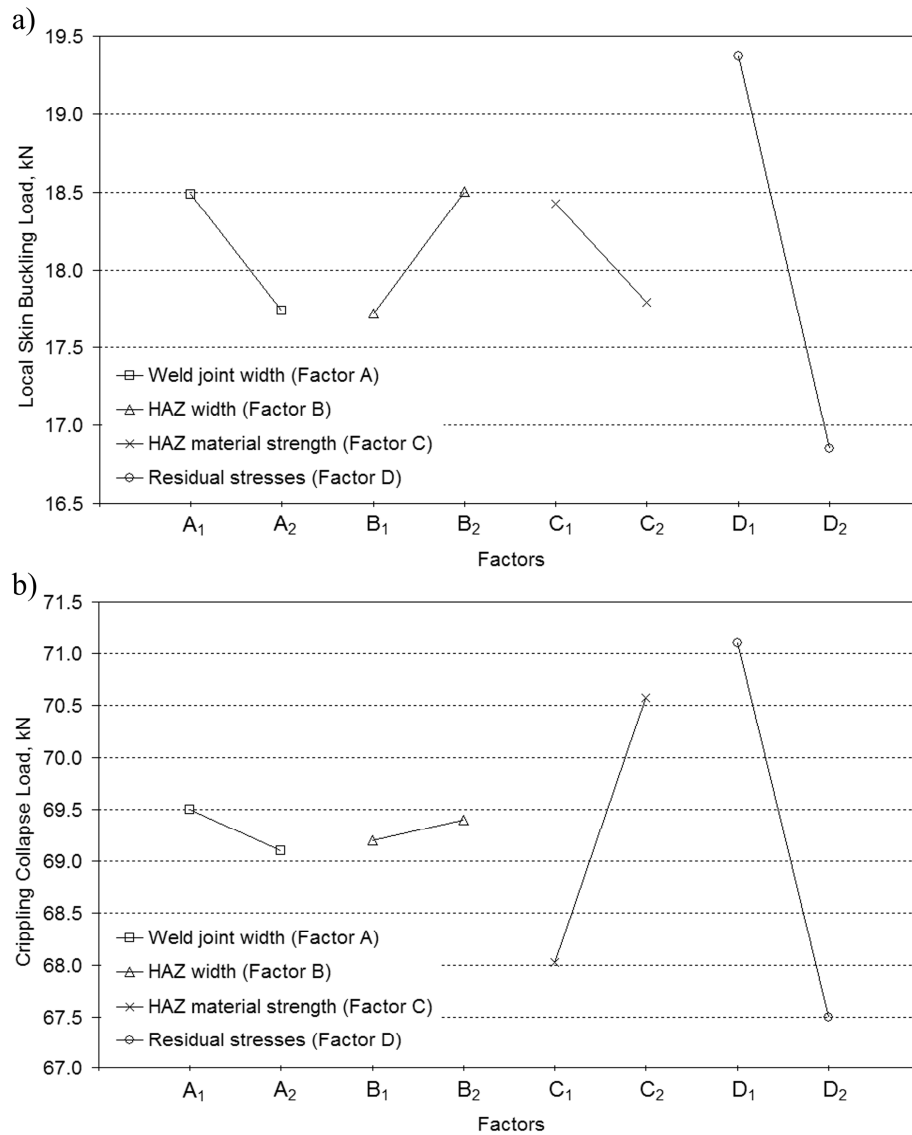
Figure 10. Dominant welding effect(s). *The graphs present the results of the Analysis of means for the welding process effects on static strength, a) Local skin buckling and b) Crippling collapse.*
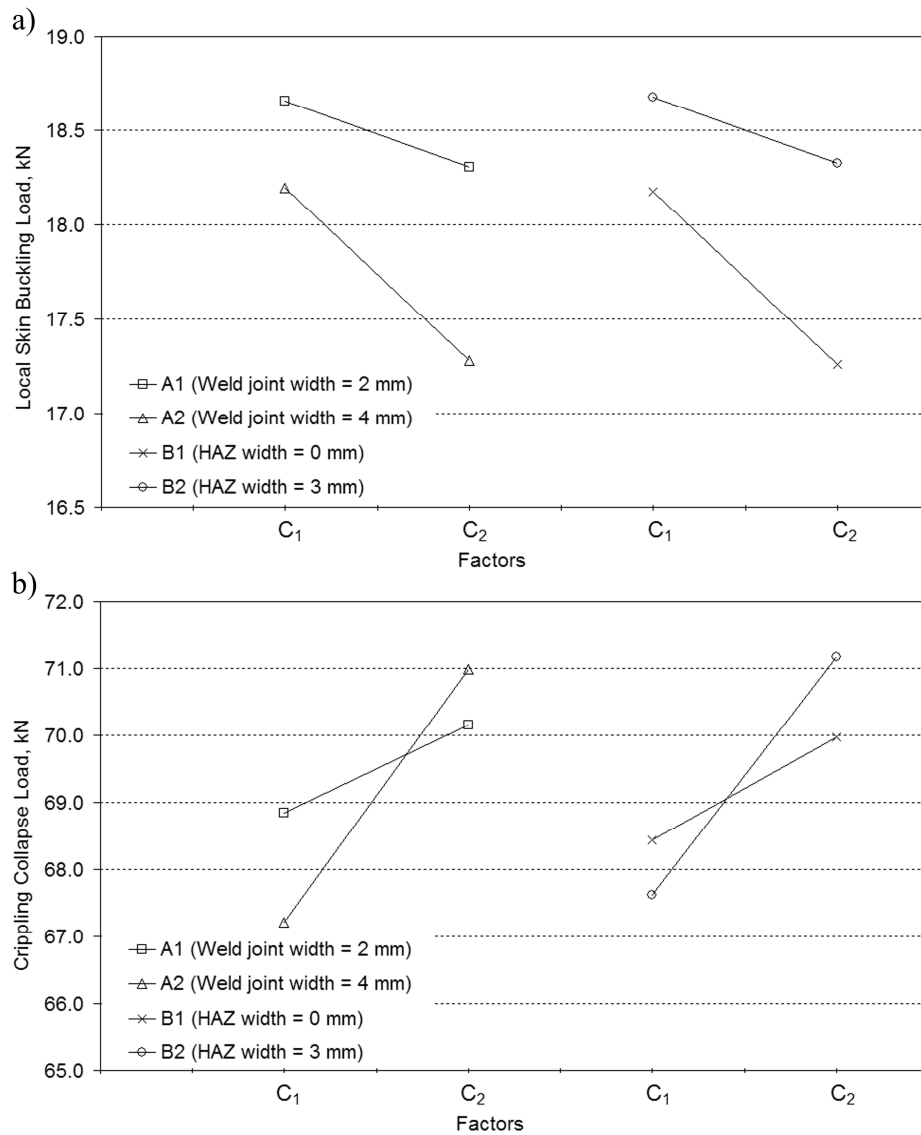
Figure 11. Interaction of welding effects. *The graphs present the results of the Analysis of means for the interaction of welding process effects on static strength, a) Local skin buckling and b) Crippling collapse.*
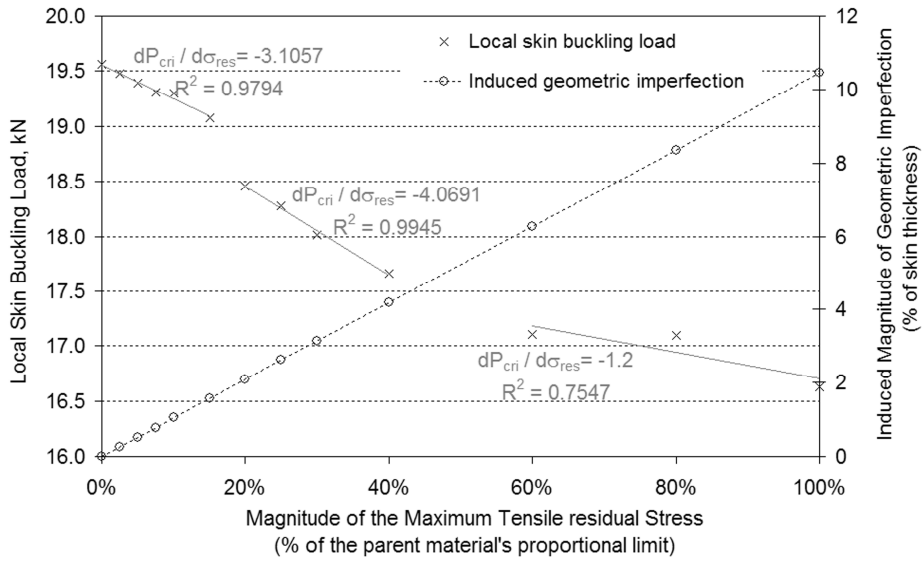
Figure 12. Local skin buckling parametric study. *The graph shows the influence of residual stress magnitude on specimen local skin buckling load.*
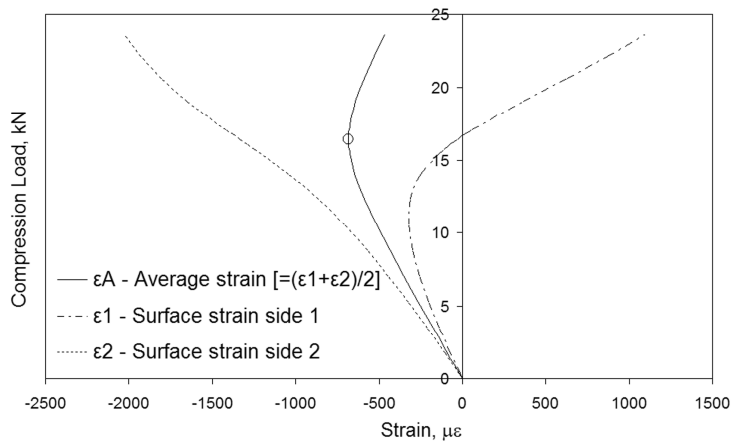

Figure 13. Local skin buckling definition. *The figure depicts a typical compression load versus mid-plane strain curve used to define local skin buckling.*
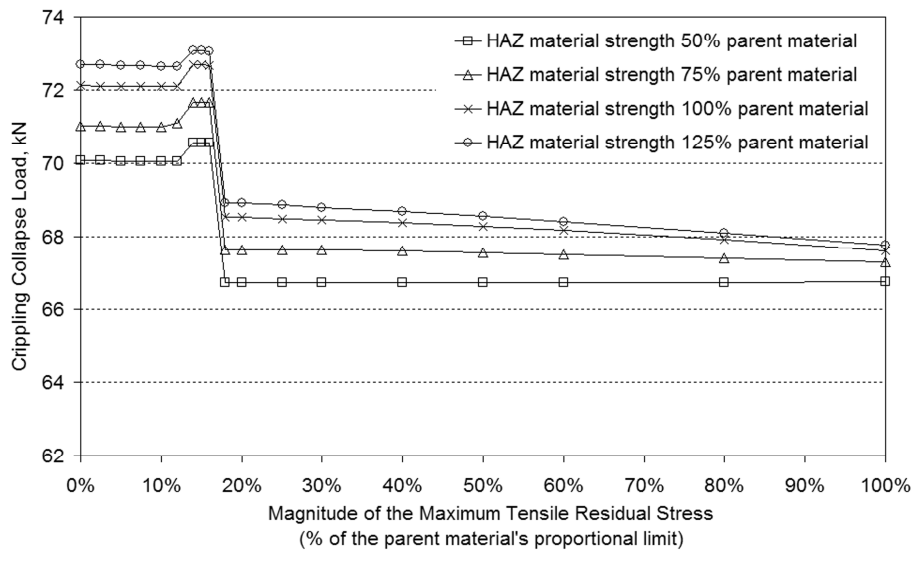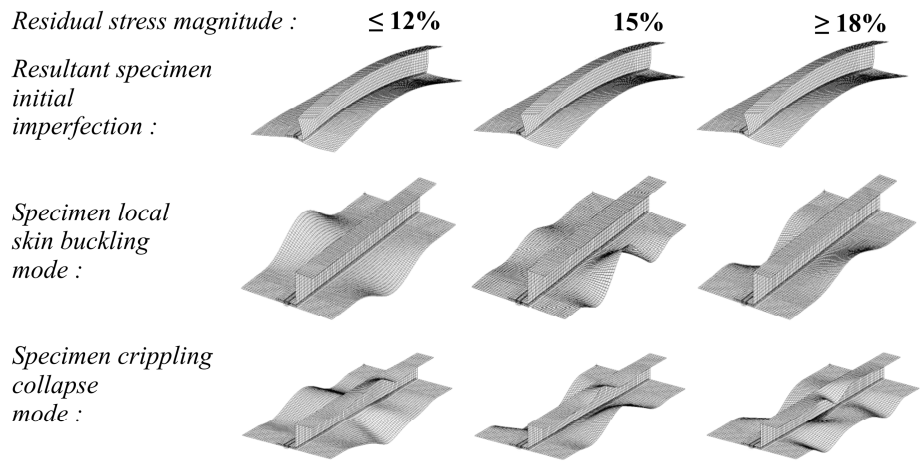
Figure 14. Crippling collapse parametric study. *The graph shows the combined influence of material strength in the HAZ and magnitude of residual stress on specimen crippling collapse load.*

Test specimen	Local skin buckling load (kN)	Specimen collapse load (kN)
FSW-1	---	73.0
FSW-2	14.0	71.7
FSW-3	---	73.4
Average	---	73.0

Table 1. Validation specimen loads. *The table documents the validation specimen local buckling and collapse loads.*

Finite Element simulation number	(Factor A) Weld joint width (mm)	(Factor C) HAZ material strength ($\%^1$)	Interaction (Factor A) x (Factor C)	(Factor B) HAZ width (mm)	(Factor D) Residual stress ($\%^2$)	Interaction (Factor B) x (Factor C)
1	2	50	1	0	0	1
2	2	50	1	3	100	2
3	2	125	2	0	0	2
4	2	125	2	3	100	1
5	4	50	2	0	100	1
6	4	50	2	3	0	2
7	4	125	1	0	100	2
8	4	125	1	3	0	1

1 – Percentage of parent material strength.
2 – Percentage of proportional limit of the HAZ material set as magnitude of welding induced tensile residual stress.

Table 2. Welding process effect orthogonal array. *The table outlines the input factors (welding process effects) for the 8 simulations undertaken to determine dominant effects on static strength.*

	Local skin buckling	Crippling collapse
	(% contribution)	(% contribution)
Factor A – Weld joint width	6.6%	0.7%
Factor B – HAZ width	7.3%	0.7%
Factor C – HAZ material strength	4.7%	26.8%
Factor D – Residual stress	74.9%	53.9%
Interaction (Factor A) x (Factor C)	0.9%	6.3%
Interaction (Factor B) x (Factor C)	0.9%	4.2%
Error	4.7%	8.1%

Table 3. Relative contributions of welding process effects. *The table outlines the relative contributions of welding process effects based on an Analysis of Variance, a) Local skin buckling and b) Crippling Collapse.*